

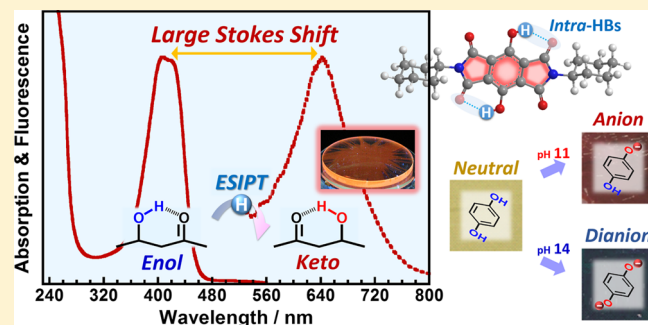
Polyimide and Imide Compound Exhibiting Bright Red Fluorescence with Very Large Stokes Shifts via Excited-State Intramolecular Proton Transfer

Kenta Kanosue, Takamichi Shimosaka, Junji Wakita, and Shinji Ando*

Department of Chemistry & Materials Science, Tokyo Institute of Technology, Ookayama 2-12-1-E4-5, Meguro-ku, Tokyo 152-8552, Japan

Supporting Information

ABSTRACT: A novel polyimide (PI) emitting a prominent red fluorescence was prepared based on 3,6-dihydroxypyromellitic dianhydride (P2HDA) and 4,4'-diaminocyclohexylmethane (DCHM). In order to investigate the fluorescence properties of the PI, an imide model compound, *N,N'*-dicyclohexyl-3,6-dihydroxypyromellitimide (P2H-Ch), corresponding to one repeating unit of the PI, was also synthesized. The UV–vis absorption and fluorescence spectra of P2H-Ch in CHCl_3 and the solid PI film demonstrated intense red fluorescence at around 640 nm with a very large Stokes shift (ν) of 7655 and 8994 cm^{-1} , respectively, via the excited-state intramolecular proton transfer (ESIPT). Moreover, the corresponding monoanion and dianion species were formed in basic conditions with an organic base (DBU) and basic salt (NaOH), which were characterized by highly visible halochromism. The introduction of $-\text{OH}$ groups into the pyromellitic moiety of imide compounds or PIs at their para positions led to the long-wavelength fluorescent emission as well as to the high pH sensitivity.



1. INTRODUCTION

Polymeric materials exhibiting fluorescent emission^{1,2} are expected to be applied for wavelength down-conversion in a wide range of applications such as flat panel displays, photovoltaic devices, and crop cultivators.^{3,4} Wavelength down-convertors can efficiently change short wavelength light (UV or violet-blue light) to longer wavelength light (green, yellow, red, or near-infrared). Polymeric fluorescent materials have attracted significant interest due to their inherent advantages, i.e., controllability of optical properties, high efficiency, light weight, flexibility, facile formation, and processing of films and thin lines by spin-coating or inkjet printing.^{5,6} However, conventional fluorescent polymers consisting of π -conjugated sequences, such as poly(phenylene vinylene) and polyfluorene derivatives, do not have sufficient thermal stability, i.e., glass transition temperatures (T_g) or degradation temperatures (T_d under air), and do not comply with the temperatures required by device fabrication processes in modern electronics and photonics applications.^{7,8} In addition, these π -conjugated polymers are generally not resistant to radiation, environmental factors, and long-term exploitation, which is also an important requirement for polymeric wavelength converting materials.

Polyimides (PIs) are a class of super engineering plastics well-known for their high thermal and chemical stability, optical and radiation resistance, and good mechanical properties originating from their rigid molecular structure and strong

intermolecular interactions. They have been widely applied in the aerospace, electrical, electronics, and photonics industries.⁹ In particular, wholly aromatic polyimides (Ar-PI) synthesized from (1) pyromellitic dianhydride and bis(4-aminophenyl) ether (PMDA/ODA) and (2) 3,3',4,4'-biphenyltetracarboxylic dianhydride and *p*-phenylenediamine (*s*-BPDA/PDA) have been commercialized as Kapton-H and Upilex-S, respectively. Recently, fluorinated PIs and semialiphatic PIs (Al-PIs) have also attracted much attention as a new class of electronic and optical materials due to their colorlessness and high transparency, low refractive index, and low birefringence.^{10–13} For example, they can be used as waveguides and optical peripheral components with highly controlled properties in the visible and near-IR region.¹¹

More recently, fluorescence properties of low-molecular-weight imide compounds,^{14–18} Ar-PIs, and Al-PIs have been widely studied.^{12,14–27} It is well-known that Ar-PIs undergo two types of electronic transitions after irradiation by UV or short-wavelength visible light.^{16,17,20,26,27} The first one is called “locally excited (LE) transition” and involves the dianhydride moieties; the second one is called “charge transfer (CT) transition” and originates from CT complex formation between electron-donating diamine and electron-accepting dianhydride

Received: December 6, 2014

Revised: February 7, 2015

moieties. Furthermore, LE transitions can be classified into “ π - π^* ” and “ n - π^* ” transitions. The LE(π - π^*) transitions in PIs are generated at π -conjugated components of the dianhydride moieties, whereas the LE(n - π^*) transitions are generated from the lone-pair electrons at the carbonyl oxygen and the nitrogen atoms of the imide rings (n -orbital). Hasegawa et al.^{19,20} first demonstrated that PMDA/ODA and *s*-BPDA/PDA PIs exhibit weak fluorescent emission at 400–700 nm in response to optical excitation at the CT absorption bands in the UV/short-visible region. However, their quantum efficiency (Φ) of CT fluorescence is very low due to the very small oscillator strengths of the CT transitions; for example, a Φ value of 9.7×10^{-7} was reported for the PMDA/ODA PI film.²¹ On the other hand, Horie et al.^{12,13} have further investigated absorption and fluorescence properties of Al-PIs based on 4,4'-diaminocyclohexylmethane (DCHM) with PMDA and 2,2-bis(3,4-dicarboxyphenyl)hexafluoropropane dianhydride (6FDA). These PIs showed high optical transparency in the visible region due to the effective suppression of intramolecular CT interactions due to the weak electron-donating property of the alicyclic diamine. However, these PIs exhibited CT emission peaks at around 500 nm in addition to the LE emission peaks at around 400 nm, although they had no apparent CT absorption peaks in the absorption spectra. The authors concluded that the CT emission was originated from the interchain CT complexes formed between the alicyclic diamine moieties of one molecular chain and the dianhydride moieties of the other. This conclusion was supported by the enhancement of CT fluorescence with increasing thermal imidization temperature. Meanwhile, Ishii et al.²⁶ have reported that an Al-PI prepared from *s*-BPDA and *trans*-1,4-diaminocyclohexane (*t*-CHDA) showed an LE absorption peak at 320 nm and an intense emission peak at 385 nm, whereas no CT absorption and fluorescence were observed. The Φ value of *s*-BPDA/*t*-CHDA was reported to be 0.05, which was much higher than that of Ar-PIs, such as PMDA/ODA. This large Φ value could be explained by the extended π -conjugation in the aromatic dianhydride moiety in addition to the suppression of intra/intermolecular CT interactions by introducing alicyclic diamine with weak electron-donating properties.

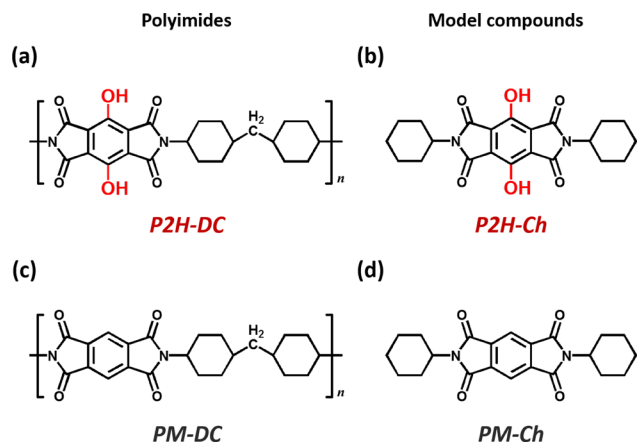
Optical measurements of imide model compounds in solution are straightforward and useful to understand and predict the fluorescence properties of PIs because PIs are generally insoluble in common organic solvents due to their rigid and linear molecular chains and strong intermolecular interactions. Recently, we have proposed and confirmed a novel molecular design concept for “highly fluorescent PIs” based on the DFT calculations and optical measurements of imide model compounds.¹⁶ The principles for designing highly fluorescent PIs can be summarized as follows: (1) use alicyclic diamines and (2) use aromatic dianhydrides that have flexible linkages with extended π -conjugation. According to this concept, we have successfully synthesized a strongly blue fluorescent Al-PI derived from 1,4-bis(3,4-dicarboxyphenoxy)benzene dianhydride (HQDEA) and DCHM, which has a Φ value of 0.11.¹⁶ We have also reported a series of Al-PIs synthesized from perfluorinated aromatic dianhydrides, such as 1,4-bis(3,4-dicarboxytrifluorophenoxy)tetrafluorobenzene dianhydride and difluoropyromellitic dianhydride, which exhibited strong bluish-green and red fluorescence, respectively.²⁵ Although their fluorescence intensity was significantly enhanced, these PIs could not be used in wavelength converters because the energy gap between the absorption and fluorescence, which corre-

sponds to the difference between the excitation and emission wavelengths called a Stokes shift, was not large enough. If much larger Stokes shift values could be achieved together with the high Φ value, UV/short-visible light from solar radiation or LED sources could be efficiently converted to yellow, orange, or red light. To significantly enhance the Stokes shift of PIs, further innovative concepts for molecular design of fluorescent PIs are demanded.

In our previous study, we reported that 3-hydroxy-*N*-cyclohexylphthalimide (3HNHPI), an imide compound containing an –OH group and forming an ideal intramolecular hydrogen bonding (*intra*-HB) between the –OH and C=O groups, exhibits strong green fluorescence with a large Stokes shift ($\nu = 11\,394\text{ cm}^{-1}$, 1.412 eV).¹⁷ It has been reported that molecules with *intra*-HB structures similar to 3HNHPI undergo excited-state intramolecular proton transfer (ESIPT) as a result of the increased proton-donating and accepting properties of –OH and C=O groups, respectively, upon excitation.^{28–30} Flavone,³¹ anthraquinone,³² quinoline,³³ benzoxazole,³⁴ and salicylidene aniline³⁵ derivatives are the representative ESIPT compounds that have been applied in laser dyes,³⁶ high-energy radiation detectors,³⁷ UV-photostabilizers,³⁸ and fluorescent probes.³⁹ In the case of 3HNHPI, the ESIPT phenomenon was strongly suggested to take place in the excited state. Excitation of an enol by UV radiation readily generates the Franck–Condon excited state, which rapidly undergoes the ESIPT process to generate an excited-state keto tautomer. During the subsequent relaxation to the ground state by radiative or nonradiative processes, a reverse proton transfer occurs to yield the original ground-state enol. Because of the large energy difference between the enol and keto tautomer, the excited-state keto tautomer exhibits an unusual green emission with a large Stokes shift. It has been reported that a wide color range of fluorescence can be generated through ESIPT processes by adjusting the relative emission intensities of enol and keto. Tang et al.⁴⁰ obtained a white-light emitting compound with a single ESIPT unit by rational tuning of the energies of the enol and the keto tautomer. In addition, polymers containing ESIPT units in their main or side chains have also been reported. Park et al.⁴¹ reported that polybenzoxazole (PBO) having two –OH groups in the repeating units exhibits an ESIPT emission at 610 nm with excitation at 380 nm ($\nu = 9939\text{ cm}^{-1}$). Chu et al.⁴² synthesized a polymer having two 2-(2'-hydroxyphenyl)-benzoxazole (HBO) moieties in the repeating unit which exhibits an ESIPT emission at 616 nm with a large Stokes shift ($\nu = 7520\text{ cm}^{-1}$). Campo et al.⁴³ reported that poly(methyl methacrylate) (PMMA) with benzazole units in its side chains exhibits various-color ESIPT emission depending on the kind of solvent or chemical structure of the benzazole moieties. However, the thermal stability of these polymers would be insufficient for optical or photonic applications due to the lower T_g of the main chains. To the best of our knowledge, thermally stable polymers such as PIs with ESIPT moieties incorporated in their main chain have never been reported.

First, 3,6-dihydroxypyromellitic dianhydride (P2HDA), which has two –OH groups in the para positions of the benzene ring of pyromellitic dianhydride, was synthesized. Additionally a PI (P2H-DC; Chart 1a) and an imide model compound (P2H-Ch; Chart 1b) were newly synthesized to examine their fluorescence properties. Comparative experiments for related molecules with the same skeleton but without –OH groups (PM-DC and PM-Ch; Chart 1c,d) were performed to clarify the substituent effect of the –OH groups

Chart 1. Chemical Structures of (a) P2H-DC, (b) P2H-Ch, (c) PM-DC, and (d) PM-Ch



and their role in the ESIPT behaviors. Second, to investigate the sensitivity of the imide compound and PI to basicity of the environment (pH), optical absorption spectra were measured in basic conditions by using an organic base (DBU) and basic salt (NaOH). This study aims to design new types of highly fluorescent PIs by introducing “ESIPT units” in the main chain, which would enable to control the absorption and fluorescence wavelength over a very wide range.

2. EXPERIMENTAL SECTION

Materials. Difluoropyromellitic dianhydride, generously supplied by NTT corporation, was used as received. Cyclohexylamine (Kanto Chemical Co., Inc.) was purified by distillation under reduced pressure. 4,4'-Diaminocyclohexylmethane (DCHM), purchased from Tokyo Kasei Kogyo Co., Ltd., was recrystallized from *n*-hexane and sublimed under reduced pressure. *N,O*-Bis(trimethylsilyl)-trifluoroacetamide ($\geq 99\%$, BSTFA, Aldrich) and *N,N*-dimethylacetamide (anhydrous, DMAc, Aldrich) were used as received. 1,8-Diazabicyclo[5.4.0]undec-7-ene (DBU, Tokyo Kasei Kogyo Co., Ltd.) was purified by distillation under reduced pressure. *o*-Xylene and sodium hydroxide (NaOH), purchased from Kanto Chemical Co., Inc., were used as received.

Synthesis. *3,6-Difluoropyromellitic Acid Tetramethyl Ester.* Difluoropyromellitic dianhydride (12.70 g, 50 mmol) was refluxed in methanol (250 mL) and concentrated sulfuric acid (7.5 mL) for 48 h. After cooling to room temperature, white powder reprecipitated by excess water was filtrated and dried. Needle-like crystals were obtained by recrystallization from methanol/water solution (yield 71%). ^1H NMR (400 MHz, DMSO- d_6 , ppm): $\delta = 3.90$ (s, 12H). ^{19}F NMR (377 MHz, DMSO- d_6 , ppm): $\delta = -116.58$. ^{13}C NMR (100 MHz, DMSO- d_6 , ppm): $\delta = 53.78, 124.12, 152.21, 161.51$. Elemental Analysis (%) Calcd for $\text{C}_{14}\text{H}_{12}\text{F}_2\text{O}_8$: C 48.56, H 3.49, F 10.97, O 36.97. Found: C 48.33, H 3.46, F 11.17, O 37.04.

3,6-Dimethoxyppyromellitic Acid Tetramethyl Ester. 3,6-Difluoropyromellitic acid tetramethyl ester (6.92 g, 20 mmol) and sodium methoxide (2.70 g, 50 mmol) dissolved in DMAc (20 mL) were heated and kept at 140 °C for 4 h under a nitrogen atmosphere. After cooling to room temperature, brown solid reprecipitated by excess water was acidified by hydrochloric acid and then filtrated and dried. Plate-like crystals were obtained by recrystallization from methanol/water solution (yield 33%). ^1H NMR (400 MHz, DMSO- d_6 , ppm) $\delta = 3.76$ (s, 6H), 3.86 (s, 12H). ^{13}C NMR (100 MHz, DMSO- d_6 , ppm) $\delta = 53.28, 64.08, 129.55, 150.63, 164.19$. Elemental Analysis (%) Calcd for $\text{C}_{16}\text{H}_{18}\text{O}_{10}$: C 51.89, H 4.90, O 43.21. Found: C 51.76, H 4.80, O 43.44.

*3,6-Dihydroxyppyromellitic Acid.*⁴⁴ 3,6-Dimethoxyppyromellitic acid tetramethyl ester (5.18 g, 14 mmol) was dissolved in a mixture of acetic acid (44 mL) and hydrobromic acid (9.56 mL) and then heated

at 100 °C for 36 h. After cooling to room temperature, yellow precipitate was filtrated and dried. Faint yellow crystals were obtained by recrystallization from water (yield 32%). ^{13}C NMR (100 MHz, DMSO- d_6 , ppm) $\delta = 121.81, 148.16, 167.91$. Elemental Analysis (%) Calcd for $\text{C}_{10}\text{H}_6\text{O}_8 \cdot 2\text{H}_2\text{O}$: C 37.28, H 3.13, O 59.59. Found: C 37.28, H 3.05, O 59.67.

P2HDA. 3,6-Dihydroxyppyromellitic acid (1.14g, 4 mmol) was heated at 180 °C under reduced pressure and resulted in yellow solid (yield 72%). ^{13}C NMR (100 MHz, acetone- d_6 , ppm) $\delta = 125.93, 147.53, 160.70$.

P2H-Ch. The precursor of P2H-Ch, amic acid silyl ester, was prepared by the *in situ* silylation method reported by Oishi et al.^{45,46} Cyclohexylamine (595 mg, 6 mmol) and BSTFA (771 mg, 3 mmol) were stirred for 30 min in DMAc (6 mL) in an ice bath (solution I). P2HDA (321 mg, 1.28 mmol) was stirred for 30 min in DMAc (6 mL) in an ice bath (solution II). Solutions I and II were mixed and then stirred overnight in an ice bath. After distillation of DMAc under reduced pressure, propionic acid (15 mL) was added and refluxed for 6 h under a nitrogen atmosphere. After cooling to room temperature, yellow solid reprecipitated by excess methanol was filtrated and dried. Yellow crystals were obtained by recrystallization from *o*-xylene (yield 72%). A melting point of P2H-Ch could not be accurately obtained due to an oxidation reaction in the -OH groups moieties at around 230 °C. ^1H NMR (400 MHz, DMSO- d_6 , ppm) $\delta = 1.1\text{--}1.4$ (m, 6H), 1.6–1.9 (m, 10H), 2.0–2.2 (m, 4H), 3.94 (m, 2H). ^{13}C NMR (100 MHz, DMSO- d_6 , ppm) $\delta = 24.13, 28.57, 49.27, 53.78, 122.95, 143.52, 164.61$. Elemental Analysis (%) Calcd for $\text{C}_{22}\text{H}_{24}\text{N}_2\text{O}_6$: C 64.07, H 5.87, N 6.79, O 23.28. Found: C 64.36, H 5.90, N 6.66, O 23.08. HRMS (EI) m/z $[\text{M} + \text{H}]^+$ calcd for $\text{C}_{22}\text{H}_{24}\text{N}_2\text{O}_6$ 412.1634; found 412.1624. The HRMS spectrum of P2H-Ch is shown in Figure S1 of the Supporting Information.

P2H-DC PI. The precursor of P2H-DC PI, poly(amic acid) silyl ester (PASE), was also prepared by the *in situ* silylation method. DCHM (84 mg, 0.4 mmol) and BSTFA (108 mg, 0.4 mmol) were stirred in DMAc (1 mL) for 30 min in an ice bath. P2HDA (100 mg, 0.4 mmol) was added to the solution and then stirred overnight. The resulting viscous yellow solution was spin-coated onto a fused silica (amorphous SiO_2) substrate, followed by soft-baking at 70 °C for 1 h and subsequent thermal imidization by a one-step imidization procedure: the final curing conditions were 220 °C for 1.5 h under nitrogen flow. The heating rate from 70 to 220 °C was 4.6 °C/min.

Measurements. Solutions of the imide compounds for optical measurements had concentrations in the range from 10^{-5} to 10^{-6} M. The solvents, chloroform (CHCl_3 , 99.9%, Kanto Chemical Co., Inc., fluorescence grade) and trifluoroacetic acid (TFA, 99.9%, Aldrich, spectroscopic grade), were used without further purification. UV/vis absorption spectra of the solutions and PI films were measured with a Hitachi U-3500 spectrophotometer. Fluorescent excitation/emission spectra of the same samples were measured with a Hitachi F-4500 fluorescence spectrometer equipped with a HAMAMATSU R928 photomultiplier tube. The fluorescence spectra of solutions were measured without degassing. The front-face method was adopted for film samples to reduce self-absorption of the emitted fluorescence. Emission spectra were measured with the excitation at the peak wavelength (λ_{ex}) of the corresponding excitation spectra. In contrast, excitation spectra were measured by monitoring the fluorescence intensity at the peak wavelength (λ_{em}) of the emission spectra. The measured spectra were not corrected for the sensitivity of the photomultiplier tubes to the fluorescence wavelength. The photoluminescence quantum efficiencies of the solution and film samples were measured in another way by using a calibrated integrating sphere (HAMAMATSU C9920) connected to a multichannel analyzer (HAMAMATSU C7473) via an optical fiber link. In this measurement, the samples were excited at a controlled λ_{ex} using a monochromated xenon light source, and the solution sample was degassed by argon prior to measurement. The single crystal of P2H-Ch was obtained from *o*-xylene solution. The single crystal XRD data of P2H-Ch was recorded on a Rigaku R-Axis RAPID-II (Cu $K\alpha$). The structure was solved by the direct methods with the program SHELXS-97 and was refined by the full-matrix least-squares method

with SHELXL-97.⁴⁷ All the non-hydrogen atoms were refined with anisotropic temperature factors. The H atoms of the –OH groups were located from the difference electron density map. The other H atoms were inserted in standard positions and refined by a riding model. The Fourier transformed infrared (FT-IR) absorption spectra of PI films were measured in the range of 650–4000 cm^{-1} using a Thermo-Fisher Avatar-320 spectrometer equipped with a Thundere-dome attenuated total reflection (ATR) attachment (incident angle 45°). The prism (internal reflection element) was made of germanium crystal with a refractive index of 4.0. All optical measurements were conducted at ambient temperature without humidity control. Thermogravimetric analysis (TGA) was conducted using a Shimadzu DTG-60 analyzer with a heating rate of 5 °C/min.

Quantum Chemical Calculation. The density functional theory (DFT) with the three-parameter Becke-style hybrid functional (B3LYP)^{48–50} was adopted for calculating electronic structures and spectroscopic properties of the imide compounds. Geometry optimization was independently performed with the 6-311G(d) basis set for the S_0 and S_1 states, respectively. The 6-311++G(d,p) basis set was used for calculating vertical excitation wavelength and oscillator strength (f) at each of the S_0 and S_1 geometries. The $S_0 \rightarrow S_1$ transition at the S_0 geometry corresponds to optical absorption of the ground state; on the other hand, that at the S_1 geometry corresponds to fluorescent emission according to Kasha's rule. All calculations were performed with the Gaussian-09 B.01 program package,⁵¹ which implements analytical gradients at the time-dependent (TD)-DFT level.

3. RESULTS AND DISCUSSION

3.1. Imide Model Compounds. Crystal Structure of P2H-Ch. The crystal structure and the details of the crystal lattice of P2H-Ch analyzed by single crystal XRD technique are shown in Figure S2 of the Supporting Information. Bilton et al.^{52–54} reported that one of the most probable intramolecular hydrogen bonding (*intra*-HB) motifs is a planar conjugated six-membered ring with a propensity for resonance-assisted hydrogen bonding (RAHB), in which short contacts are formed between hydrogen donors and acceptors. P2H-Ch apparently has a typical RAHB structure in which electrons alleviate the bias of charges by the resonance, which is well demonstrated by the short distances between the atoms forming a pair of *intra*-HBs: H1–O6 (2.240(2) Å) and O2–O6 (2.941(2) Å) and a typical angle O2–H1–O6 (140(2)°).

UV/Vis Absorption and Fluorescence Spectra of the Imide Compounds. First, the fluorescence properties of solutions of the imide model compounds, PM-Ch and P2H-Ch, were examined to clarify the effects of the –OH groups. The UV/vis absorption and fluorescence excitation/emission spectra of PM-Ch and P2H-Ch dissolved in CHCl_3 (1×10^{-5} M) are shown in Figures 1, 2a, and 2b, respectively. Table 1 summarizes the peak wavelengths in the optical absorption (λ_{abs}) and excitation/emission (λ_{ex} , λ_{em}) spectra, the Stokes shifts (ν), and photoluminescence quantum efficiencies (Φ) observed for these solutions. The calculated vertical excitation wavelengths, oscillator strengths (f), contributing molecular orbitals (MO), assignment of the electronic transitions, and the contribution of each transition for the compounds at the S_0 geometry are listed in Table 2. Here, HOMO– m and LUMO+ m denote the ($m + 1$)-th highest occupied MO and the ($m + 1$)-th lowest unoccupied MO, respectively. In addition, the calculated emission wavelengths ($\lambda_{\text{em,cal}}$) and the assignment of electronic transitions for the compounds in the excited state with the optimized S_1 geometry are listed in Table S1 of the Supporting Information.

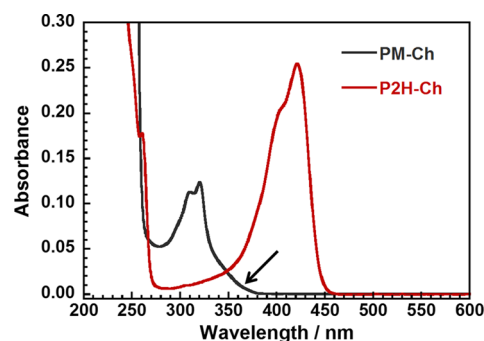


Figure 1. Optical absorption spectra of PM-Ch and P2H-Ch (1×10^{-5} M) in CHCl_3 solution. The arrow denotes a weak absorption tailing of PM-Ch solution.

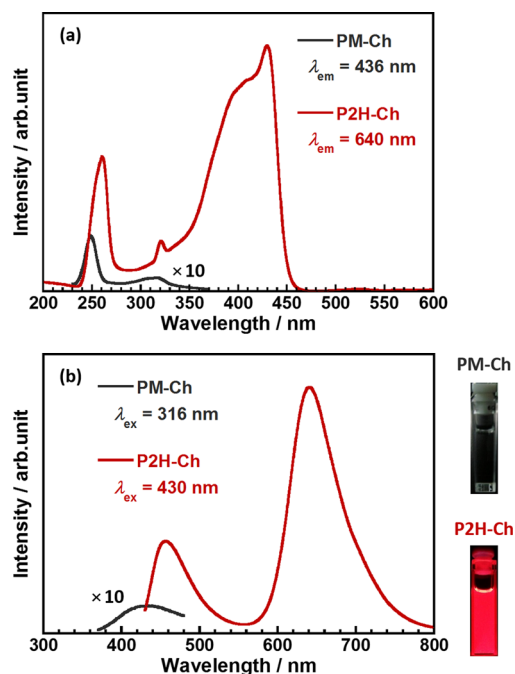


Figure 2. Fluorescence spectra of PM-Ch and P2H-Ch (1×10^{-5} M) in CHCl_3 solution: (a) excitation spectra monitored at λ_{em} ; (b) emission spectra excited at λ_{ex} and photo images of these solutions under UV ($\lambda = 365$ nm) irradiation.

Table 1. Experimental Absorption Wavelengths (λ_{abs}), Excitation/Emission Wavelengths (λ_{ex} , λ_{em}), Stokes Shifts (ν), and Photoluminescence Quantum Efficiencies (Φ) of PM-Ch and P2H-Ch (1×10^{-5} M) in CHCl_3 Solutions

imide compound	λ_{abs} (nm)	λ_{ex} (nm)	λ_{em} (nm)	ν^a (cm^{-1})	Φ
PM-Ch	320	316	436	8710 ^b	<0.01
P2H-Ch	421	430	457, 641	1374, 7655	0.16

^a $\nu = 10^7 (1/\lambda_{\text{ex}} - 1/\lambda_{\text{em}})$. ^bIn the case of PM-Ch, λ_{abs} and λ_{ex} are not corresponding to $S_0 \rightarrow S_1$ but $S_0 \rightarrow S_2$ transition wavelength.

As shown in Figure 1, PM-Ch, an OH-free imide compound, not forming *intra*-HB, exhibits an absorption peak at 320 nm with a weak tailing at around 360 nm (depicted by an arrow). The spatial distributions of the calculated MOs are illustrated in Figure S3 of the Supporting Information. The HOMO–3 of PM-Ch, which is localized around the lone pair of electrons of the oxygen and nitrogen atoms of the imide rings, is a

Table 2. Calculated Electronic Transitions of PM-Ch and P2H-Ch at the Optimized S_0 Geometry^a

imide compound	state	transition wavelength (nm)	oscillator strength	orbitals		character of transition	contribution	
PM-Ch	S_1	356.6	0.0001	HOMO-1	→	LUMO	$n-\pi^*$	0.95
				HOMO-3	→	LUMO+2	$n-\pi^*$	0.05
	S_2	348.9	0.0023	HOMO	→	LUMO	$\pi-\pi^*$	1.00
	S_7	291.7	0.0391	HOMO-5	→	LUMO	$\pi-\pi^*$	0.76
				HOMO	→	LUMO+1	$\pi-\pi^*$	0.18
P2H-Ch enol	S_1	412.7	0.2368	HOMO-7	→	LUMO+1	$\pi-\pi^*$	0.06
				HOMO	→	LUMO	$\pi-\pi^*$	1.00
	S_2	371.3	0.0001	HOMO-2	→	LUMO	$n-\pi^*$	0.97
	S_3	357.6	0.0024	HOMO-4	→	LUMO+1	$n-\pi^*$	0.03
				HOMO-1	→	LUMO	$\pi-\pi^*$	1.00
P2H-Ch keto	S_1	557.9	0.2329	HOMO	→	LUMO	$\pi-\pi^*$	1.00
	S_3	386.9	0.0012	HOMO-2	→	LUMO	$\pi-\pi^*$	0.98
				HOMO-3	→	LUMO	$\pi-\pi^*$	0.02
	S_4	362.5	0.0001	HOMO-4	→	LUMO	$n-\pi^*$	0.97
				HOMO-1	→	LUMO+1	$n-\pi^*$	0.03

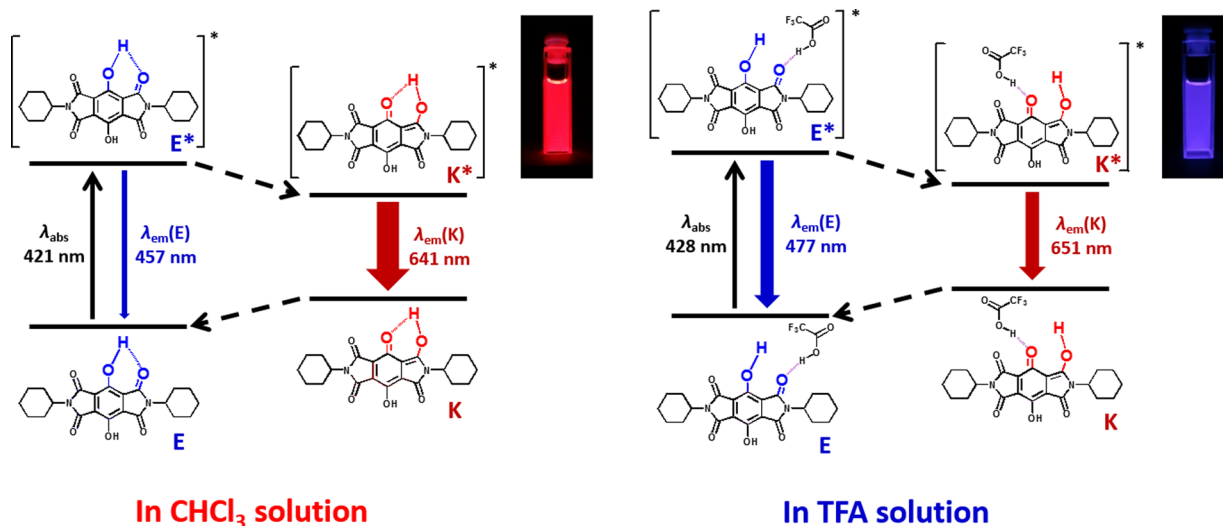
^aProhibited transitions ($f = 0$) are not listed.

nonbonding (n) orbital, and the HOMO, LUMO, LUMO+1, and LUMO+2, which are delocalized over the dianhydride moiety, are π orbitals. Accordingly, the calculated transition at 356.6 nm ($S_0 \rightarrow S_1$) is assignable to an $LE(n-\pi^*)$, and those at 348.9 nm ($S_0 \rightarrow S_2$) and 291.7 nm ($S_0 \rightarrow S_7$) are assignable to an $LE(\pi-\pi^*)$ transition (Table 2). The wavelength of the $S_0 \rightarrow S_1$ transition with a small f value (0.0001) agrees well with the weak absorption tailing at longer wavelengths in the experimental absorption spectrum (around 360 nm), in which the weak tailing is attributable to the $LE(n-\pi^*)$ band. In contrast, the experimental absorption peak (320 nm) is in agreement with the calculated $S_0 \rightarrow S_2$ transition with a relatively large f value (0.0023), which indicates that this peak is attributable to the $LE(\pi-\pi^*)$ band. The excitation and emission peaks of PM-Ch are observed at 316 and 436 nm, respectively, as shown in Figure 2. The excitation peak is attributable to an $LE(\pi-\pi^*)$ band because its wavelength (λ_{ex}) is in agreement with that of the $LE(\pi-\pi^*)$ band in the absorption spectrum (320 nm). When PM-Ch in $CHCl_3$ is excited at 316 nm, a fast internal conversion from the Franck-Condon S_2 states to the lowest energy S_1 state takes place (Table 2). Hence, the emission peak at 436 nm is attributable to an $LE(n-\pi^*)$ fluorescence, which is verified by the fact that λ_{em} agrees well with the calculated wavelength of the $LE(n-\pi^*)$ emission (440.2 nm, see Table S1 of the Supporting Information). Since the f values for $LE(n-\pi^*)$ transitions are generally very small, the $LE(n-\pi^*)$ fluorescence of PM-Ch is too weak to be seen with the eyes ($\Phi < 0.01$) as demonstrated by the photo image in Figure 2b.

In contrast, P2H-Ch, which can form *intra*-HBs, dissolved in $CHCl_3$, displays an intense absorption peak at 421 nm with a shoulder at 400 nm (Figure 1). This peak is unambiguously attributable to the $LE(\pi-\pi^*)$ band of the enol because it has a calculated value of 412.7 nm ($S_0 \rightarrow S_1$) with a very large f value (0.2368). This intense absorption peak shows a significant bathochromic shift compared to PM-Ch, which is explainable by the electron donating effects of the two $-OH$ groups in the para-positions of P2H-Ch. A similar phenomenon was also observed for 2,6-dihydroxynaphthalene carbaldehyde which also has two *intra*-HBs.⁵⁵ We have reported that introduction of an *intra*-HB into the anhydride moiety of imide compounds effectively lowers the energy level of the n orbital, and then the $S_0 \rightarrow S_1$ transition becomes an $LE(\pi-\pi^*)$ transition, not an

$LE(n-\pi^*)$ transition. This leads to a significant enhancement of the fluorescent intensity of the LE emission from the π^* orbital.¹⁷ For example, the HOMO-1 of PM-Ch, which is assignable to an n orbital, is stabilized to a lower energy state (HOMO-2) in P2H-Ch by the introduction of $-OH$ groups (see Figure S3 of the Supporting Information). Moreover, it is very likely that P2H-Ch forms dual *intra*-HBs in solution as well as in crystalline state, which also stabilizes the n orbitals, leading to a decrease in the $LE(\pi-\pi^*)$ transition energy relative to that for $LE(n-\pi^*)$.^{56,57}

For P2H-Ch dissolved in $CHCl_3$, dual fluorescent emission peaks are observed at 457 and 641 nm upon excitation at 430 nm. These peaks demonstrate relatively small (1374 cm^{-1} , 0.17 eV) and very large Stokes shifts (7655 cm^{-1} , 0.95 eV), respectively. The electronic transition caused by excitation is attributable to the lowest energy $LE(\pi-\pi^*)$ transition of the enol because the λ_{ex} value agrees well with that of the $LE(\pi-\pi^*)$ absorption band (421 nm). The first light-blue fluorescence peak at 457 nm is attributable to the $LE(\pi-\pi^*)$ fluorescence from the enol because the λ_{em} value is close to the calculated value (454.4 nm; see Table S1 of the Supporting Information). In contrast, the bright red fluorescence peak at 641 nm with the large Stokes shift should be emitted via a photophysical process with excited-state intramolecular proton transfer (ESIPT) caused by excitation at 430 nm. The occurrence of ESIPT in the excited state can be verified by the following facts. First, the calculated λ_{em} of the keto tautomer (630.3 nm, see Table S1 of the Supporting Information) is comparable to the experimental value (640 nm). Second, P2H-Ch forms six-membered-ring planar structures with *intra*-HBs in the ground state, which are typical RAHB structures (see Figure S2 of the Supporting Information). Similar structure is frequently found in ESIPT compounds.²⁸⁻³⁰ Up to now, several molecules with a structure similar to P2H-Ch have been reported to exhibit ESIPT emission. Hanson et al.⁵⁸ reported that a 1,3-bis(2-pyridylimino)isoindoline (BPI) derivative containing $-OH$ groups exhibits an ESIPT emission peak at 597 nm with a large Stokes shift (6600 cm^{-1} , 0.82 eV) in a CH_2Cl_2 solution. Fin et al.⁵⁹ reported that a naphthalenediimide derivative containing $-OH$ groups exhibits dual emission peaks at 500 and 630 nm in a DMSO/water 4:1 solution, and the latter band was attributed to an ESIPT emission. Third, the relative

Scheme 1. Schematic Representation of Excitation and Emission Mechanism with ESIPT Photocycle Scheme of P2H-Ch in CHCl_3 and TFA Solutions


intensity of the emission peaks at 477 and 651 nm in a TFA solution is much larger than that in a CHCl_3 solution (see Figure S4 of the Supporting Information). Because of the strong hydrogen-donating property of TFA, *intra*-HBs in P2H-Ch were destroyed, and the ESIPT process was suppressed because of the formation of *inter*-HBs with TFA. Roberts and co-workers⁶⁰ investigated the effect of solvents on the ESIPT emission of 2-(2'-hydroxyphenyl)benzimidazole (HBI). With increasing concentrations of trifluoroethanol (TFE), which has strong hydrogen-donating properties, the emission originating from the keto tautomer at 470 nm gradually faded out producing of a weak emission band between 350 and 400 nm. This emission band was attributed to the enol, which forms *inter*-HBs with TFE. In our previous report,¹⁷ the emission from the enol of 3-hydroxy-*N*-cyclohexylphthalimide (3HNPPI) having an ESIPT property was observed in its TFA solution. In the case of P2H-Ch, which has a structure similar to 3HNPPI, suppression of the proton transfer in the excited state in TFA should occur in a similar manner. The emission peak at 641 nm in CHCl_3 is readily attributable to the excited-state keto tautomer formed as a result of the ESIPT process. The Φ value of 0.16 is significantly larger than that of PM-Ch ($\Phi < 0.01$), which mainly originates from the very large f value (0.2329) of $\text{LE}(\pi-\pi^*)$ transition ($S_0 \rightarrow S_1$) of the keto tautomer of P2H-Ch. The expected photophysical behavior of the compounds under investigation in the CHCl_3 and TFA solutions is illustrated in Scheme 1. It is obvious that the prominent red emission observed in CHCl_3 solution is generated via the ESIPT process, whereas the light-blue emission of the TFA solution is due to the prohibition of ESIPT by the formation of *inter*-HBs with solvent molecules.

Variations in Absorption Spectra under Basic Conditions. The pK_a of phenolic $-\text{OH}$ groups is generally lower than that of alkyl alcohol $-\text{OH}$ groups. This is due to the resonance effect with the neighboring aromatic rings, which effectively stabilizes the conjugate base of the phenolic compounds. Therefore, deprotonation of $-\text{OH}$ groups easily occurs in the presence of basic reagents (e.g., NaOH and DBU). It is also well known that hydroquinone derivatives can be in a monoanion or dianion form depending on pH.^{59,61} Zahid et al.⁶¹ reported the absorption properties of 2,3,5,6-tetracyano-

1,4-hydroquinone (TCHQ) under conditions with various pH using citric acid and Na_2HPO_4 aqueous solutions. Under pH 2 and 8, absorption peaks attributed to its monoanion and dianion forms were newly observed at 461 and 520 nm, respectively. Since P2H-Ch can form a hydroquinonoid structure, its UV/vis absorption spectrum can change depending on the basic conditions. In this study, DBU dissolved in CHCl_3 was used to adjust the basicity of the solutions. Figure 3

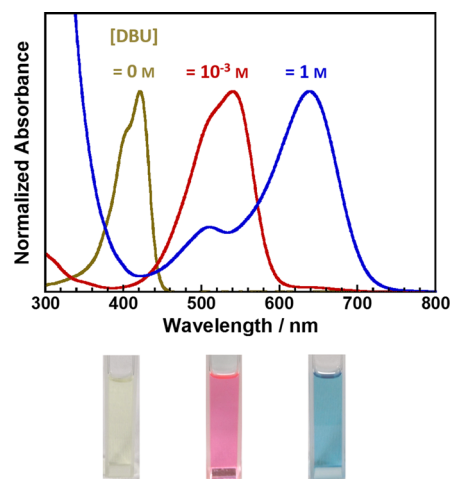


Figure 3. Optical absorption spectra of P2H-Ch (1×10^{-5} M) under basic conditions using CHCl_3 /DBU mixed solvents.

shows variations in absorption spectra of P2H-Ch depending on the DBU concentration ($[\text{DBU}]$). When $[\text{DBU}]$ reached 10^{-3} M, the color of the solution immediately changed from pale yellow to bright pink. In addition, a new strong absorption peak was observed at 540 nm while the original absorption band at 421 nm disappeared. This spectral change clearly indicates that deprotonation was promoted by DBU, and the new absorption band is attributed to the monoanion form. Furthermore, when $[\text{DBU}]$ is increased up to 1 M, the color of the solution gradually changed from bright pink to light blue. In addition, another new absorption peak was observed at a much longer wavelength (638 nm), and the band at 540 nm

significantly weakened. This indicates that the second deprotonation step took place, and the new absorption band is attributable to the dianion form. As seen in the photos in Figure 3, the pH-dependent color change, i.e., halochromism, from pale yellow (enol, neutral) to light blue (dianion) through bright pink (monoanion) is very vivid and prominent. These results clearly indicate that the introduction of $-OH$ groups into imide compounds make them more sensitive to a basic environment.

3.2. Highly Fluorescent PI Containing $-OH$ Groups.

Characterizations of the PIs. The ATR FT-IR spectra of the PM-DC and P2H-DC films are shown in Figure S5 of the Supporting Information. The completion of thermal imidization was confirmed by the $C=O$ and $C-N$ stretching bands of the imide rings at 1700 and 1360 cm^{-1} , respectively. Notably, the $C=O$ stretching peak of P2H-DC is significantly shifted to a lower wavenumber by 8 cm^{-1} relative to that of PM-DC, which could be caused by the formation of *intra*-HBs between the phenolic $-OH$ and imide $C=O$ groups in P2H-DC.^{17,54} The decomposition temperatures at a 5% weight loss (T_d^5) for PM-DC and P2H-DC were found to be 462 and $364\text{ }^\circ\text{C}$, respectively. The TGA curve of P2H-DC is shown in Figure S6 of the Supporting Information. Despite the lower T_d^5 temperature for P2H-DC, which may be due to the intermolecular dehydration reaction at the phenolic $-OH$ moiety, both PIs demonstrated good thermal stability without significant weight losses below $350\text{ }^\circ\text{C}$. The high thermal stability of the PIs originating from the rigid molecular structure without degradable side chains is preferable and advantageous for fabrication processes in modern electronics and photonics applications.

UV/Vis and Fluorescence Spectra of the PI Films. The UV/vis absorption spectra of the PM-DC and P2H-DC solid films are shown in Figure 4. These PI films exhibit absorption bands

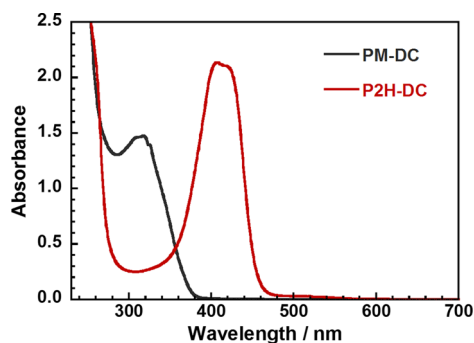


Figure 4. Optical absorption spectra of PM-DC and P2H-DC PI films.

with peak maxima at 317 and 407 nm , respectively. These peaks coincide well with those of the corresponding imide model compounds (320 nm for PM-Ch and 421 nm for P2H-Ch), indicating that the PIs have electronic structures similar to the model compounds in the ground states. Accordingly, both of the absorption peaks are readily attributable to the $LE(\pi-\pi^*)$ bands. Figure 5 represents photo images of the PM-DC and P2H-DC films under white light exposure (left side). The highly transparent colorless PM-DC film shows only a weak absorption peak at 317 nm with its main absorption peak being in the UV region, whereas the P2H-DC film is pale yellow in color and has an absorption peak with a maxima at 407 nm , a shoulder at 418 nm , and a tailing up to 500 nm (Figure 4). The long wavelength shift of the absorption band of P2H-DC

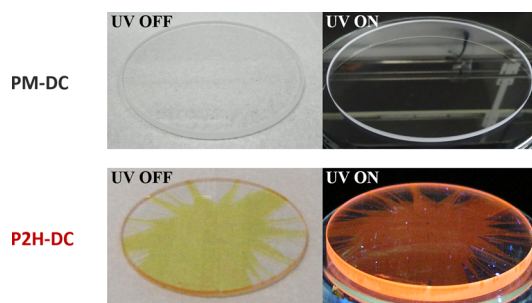


Figure 5. Photo images of PM-DC and P2H-DC PI films under white light (left) and UV ($\lambda = 365\text{ nm}$) irradiation (right).

relative to PM-DC (by 90 nm) is comparable to that of P2H-Ch and PM-Ch (by 101 nm). Note that the shoulder peak of the PI (P2H-DC) is located at a slightly shorter wavelength than the main peak of the imide model compound (P2H-Ch), although the area of the absorption band in the visible region for the PI is larger than that for the model compound.

Figure 6 shows the fluorescence spectra of the PM-DC and P2H-DC films, in which relatively wide bands of fluorescent

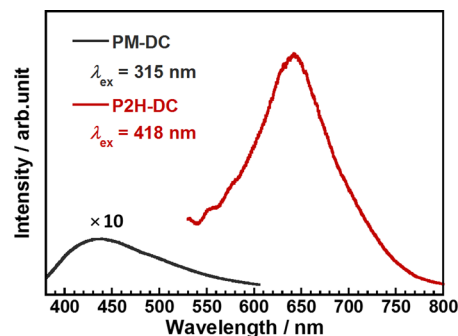


Figure 6. Fluorescence spectra of PM-DC and P2H-DC PI films.

emission are observed at 439 and 642 nm as a result of excitation at 315 and 418 nm , respectively. These bands also coincide well with the emission bands of PM-Ch and the keto form of P2H-Ch (440 and 630 nm , respectively) dissolved in CHCl_3 (Figure 2b and Table 1). The intense red emission band of P2H-DC clearly indicates that, even in the solid state, ES IPT is a dominant process in the excited state of the PI and causes a very large Stokes shift (8994 cm^{-1} , 1.12 eV). This value is comparable with the Stokes shifts of benzoxazole-type ES IPT polymers.^{41,42} Although dual emission peaks from the enol and keto forms were observed at 457 and 641 nm for P2H-Ch in solution, the emission from the enol form was not clearly observed for P2H-DC due to overlap with the excitation radiation (not shown). As seen in Figure 5 (right), the P2H-DC film exhibits prominent red fluorescent emission under UV light irradiation (LED light source at 365 nm). The Φ value of P2H-DC was not so high (0.01), though this value is significantly enhanced compared with conventional PIs such as PMDA/ODA ($\Phi = 9.7 \times 10^{-7}$). These results clearly demonstrate that ES IPT can be efficiently induced upon excitation of the solid PI films, producing a significantly large Stokes shift. The ES IPT phenomenon is a powerful and versatile tool to control the fluorescence wavelengths and Stokes shifts of imide compounds and PIs.

Variations in the Optical Absorption Properties of the P2H-DC Film under Basic Conditions. Figure 7 shows the UV/

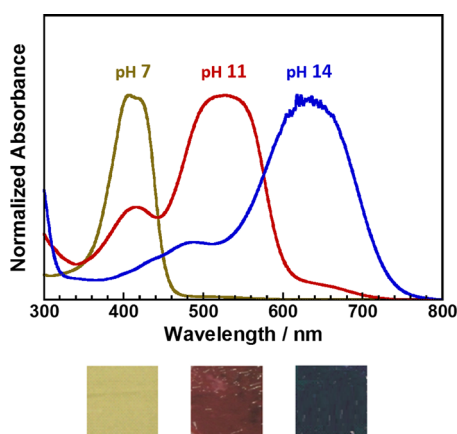


Figure 7. Optical absorption spectra of P2H-DC PI film under basic conditions using various concentrated NaOH(aq).

vis absorption spectra of the P2H-DC film under basic conditions. The spectra were measured after soaking the PI film in NaOH aqueous solutions (pH 11 and 14). Variations of the absorption spectra with the elapsed time are shown in Figure S7 of the Supporting Information. At pH 11, the intensity of the absorption band at 407 nm for P2H-DC gradually decreased and the intensity of the new band at 529 nm increased. The wavelength of the new band agrees well with the absorption band of P2H-Ch dissolved in CHCl_3/DBU ($[\text{DBU}] = 10^{-3} \text{ M}$), indicating that the band is attributable to the monoanion form of P2H-DC. After soaking in a basic solution, the film color gradually changed from pale yellow to deep red due to the first deprotonation of the $-\text{OH}$ group in the dianhydride moiety. Furthermore, at pH 14, another new absorption band was observed at a much longer wavelength around 630 nm. This also agrees well with the absorption band of P2H-Ch dissolved in CHCl_3/DBU ($[\text{DBU}] = 1 \text{ M}$), indicating that the new band is attributable to the dianion form of P2H-DC. The film color then changed to deep blue due to the second deprotonation of the residual $-\text{OH}$ groups. These facts indicate that PIs with $-\text{OH}$ groups at the pyromellitic moiety are also sensitive to the basic conditions even in the solid state, exhibiting significant halochromism. Therefore, the highly fluorescent PIs derived from P2HDA can be potential candidates for the innovative wavelength converting materials which can convert short wavelength light to long wavelength light with high efficiency. In addition, they can be used not only in electronics and photonics applications, but also as pH sensors with color changes from yellow through deep red (at pH 11) to deep blue (pH 14).

4. CONCLUSION

A highly fluorescent PI and imide compound emitting prominent red fluorescence at long wavelengths were rationally designed and synthesized. Two $-\text{OH}$ groups were introduced to the pyromellitic dianhydride moiety of the compounds to form *intra*-HBs with the imide $\text{C}=\text{O}$ groups. To investigate the effects of the introduced $-\text{OH}$ groups, fluorescence properties of the PIs and imide compounds with the same structure but without $-\text{OH}$ groups were compared. In CHCl_3 solutions, only a weak $\text{LE}(n-\pi^*)$ fluorescence peak was observed for PM-Ch ($\Phi < 0.01$), whereas an intense $\text{LE}(\pi-\pi^*)$ fluorescence peak was observed for P2H-Ch ($\Phi = 0.16$). The $-\text{OH}$ groups in P2H-Ch significantly lower the transition

energy of the $\text{LE}(\pi-\pi^*)$ transition and enhance the LE fluorescence from the π^* orbital. In addition, P2H-Ch, which forms *intra*-HBs, exhibited a strong emission from the excited keto-form at 641 nm with a very large Stokes shift (7655 cm^{-1}) via the ESIPT process. Under basic conditions prepared by mixed solvents of CHCl_3/DBU , the UV/vis absorption spectrum of P2H-Ch was significantly altered in response to $[\text{DBU}]$. Strong absorption peaks appeared at 540 and 638 nm at $[\text{DBU}] = 10^{-3}$ and 1 M and are attributable to monoanion and dianion forms resulting from the first and second deprotonations, respectively.

The novel highly fluorescent PI, P2H-DC, also exhibited prominent red emission at 642 nm with a very large Stokes shift of 8994 cm^{-1} due to the efficient ESIPT process in the solid state. In addition, the thermal degradation temperature of the PI exceeds $350 \text{ }^\circ\text{C}$. After soaking in NaOH aqueous solutions at pH 11 and 14, intense absorption peaks corresponding to the monoanion and dianion forms of P2H-DC were observed at 529 and 617 nm, respectively. It was verified that rational introduction of $-\text{OH}$ groups into the PI and imide compound enabled to generate and control the characteristic red fluorescence, its high sensitivity to basic conditions, and visible halochromism. This study proposes a new molecular design concept for enhancement and control of the fluorescence properties of PIs and imide compounds based on the ESIPT phenomenon. The highly red fluorescent PIs derived from P2HDA are promising for new electronics and photonics applications as well as for the manufacture of wavelength converters and pH sensors.

■ ASSOCIATED CONTENT

Supporting Information

HRMS spectrum of P2H-Ch, single-crystal XRD data for P2H-Ch, calculated molecular orbitals of PM-Ch and P2H-Ch (TD-DFT method at the B3LYP/6-311++G(d,p) level), absorption and fluorescence spectra of P2H-Ch in a TFA solution, ATR FT-IR spectra of PM-DC and P2H-DC film, TGA curve of the P2H-DC film, and elapsed time variations of the absorption spectra of P2H-DC soaked in NaOH aqueous solutions at pH 11 and 14; X-ray crystallographic information file (CIF) of the crystal structure of P2H-Ch. This material is available free of charge via the Internet at <http://pubs.acs.org>.

■ AUTHOR INFORMATION

Corresponding Author

*E-mail: sando@polymer.titech.ac.jp (S.A.).

Notes

The authors declare no competing financial interest.

■ ACKNOWLEDGMENTS

Single-crystal XRD data for P2H-Ch were collected and analyzed by Dr. Kohei Johmoto and Prof. Hidehiro Uekusa at Tokyo Institute of Technology. Their cooperation and efforts are greatly acknowledged.

■ REFERENCES

- Holmes, A. B.; Bradley, D. D. C.; Brown, A. R.; Burn, P. L.; Burroughes, J. H.; Friend, R. H.; Greenham, N. C.; Gymer, R. W.; Halliday, D. A.; Jackson, R. W.; Kraft, A.; Matrtens, J. H. F.; Pichler, K.; Samuel, I. D. W. *Synth. Met.* **1993**, *55–57*, 4031–4040.
- Chen, S. A.; Jen, T. H.; Lu, H. H. *J. Chin. Chem. Soc.* **2010**, *57*, 439–458.
- Geffroy, B.; Roy, P.; Prat, C. *Polym. Int.* **2006**, *55*, 572–582.

- (4) Thomas, C. P.; Wedding, A. B.; Martin, S. O. *Sol. Energy Mater. Sol. Cells* **2012**, *98*, 455–464.
- (5) Haque, S. A.; Kooops, S.; Tokmoldin, N.; Durrant, J. R.; Huang, J.; Bradley, D. D. C.; Palomares, E. *Adv. Mater.* **2007**, *19*, 683–687.
- (6) Satoh, R.; Naka, S.; Shibata, M.; Okada, H.; Onnagawa, H.; Miyabayashi, T.; Inoue, T. *Jpn. J. Appl. Phys.* **2004**, *43*, 7725–7728.
- (7) Vak, D.; Jo, J.; Ghim, J.; Chun, C.; Lim, B.; Heeger, A. J.; Kim, D. Y. *Macromolecules* **2006**, *39*, 6433–6439.
- (8) Liu, J.; Zou, J.; Yang, W.; Wu, H.; Li, C.; Zhang, B.; Peng, J.; Cao, Y. *Chem. Mater.* **2008**, *20*, 4499–4506.
- (9) Sroog, C. E. *J. Polym. Sci., Macromol. Rev.* **1976**, *11*, 161–208.
- (10) Reuter, H.; Franke, H.; Feger, C. *Appl. Opt.* **1988**, *27*, 4565–4571.
- (11) Matsuura, T.; Ando, S.; Sasaki, S.; Yamamoto, F. *Macromolecules* **1994**, *27*, 6665–6670.
- (12) Li, Q.; Horie, K.; Yokota, R. *J. Photopolym. Sci. Technol.* **1997**, *10*, 49–54.
- (13) Lee, S. A.; Yamashita, T.; Horie, K. *J. Polym. Sci., Part B: Polym. Phys.* **1998**, *36*, 1433–1442.
- (14) Creed, D.; Hoyle, C. E.; Jordan, J. W.; Pandey, C. A.; Nagarajan, R.; Pankasem, S.; Peeler, A. M.; Subramanian, P. *Macromol. Symp.* **1997**, *116*, 1–13.
- (15) Huang, W.; Yan, D.; Lu, Q. *Polym. Bull.* **2003**, *49*, 417–423.
- (16) Wakita, J.; Sekino, H.; Sakai, K.; Urano, Y.; Ando, S. *J. Phys. Chem. B* **2009**, *113*, 15212–15224.
- (17) Wakita, J.; Inoue, S.; Kawanishi, N.; Ando, S. *Macromolecules* **2010**, *43*, 3594–3605.
- (18) Demeter, A. *React. Kinet. Catal. Lett.* **2005**, *85*, 331–339.
- (19) Hasegawa, M.; Kochi, M.; Mita, I.; Yokota, R. *Eur. Polym. J.* **1989**, *25*, 349–354.
- (20) Hasegawa, M.; Horie, K. *Prog. Polym. Sci.* **2001**, *26*, 259–335.
- (21) Arjavalangam, G.; Hougham, G.; LaFemina, J. P. *Polymer* **1990**, *31*, 840–844.
- (22) Wu, A.; Akagi, T.; Jikei, M.; Kakimoto, M.; Imai, Y.; Ukishima, S.; Takahashi, Y. *Thin Solid Films* **1996**, *273*, 214–217.
- (23) Li, W.; Fox, M. A. *J. Phys. Chem. B* **1997**, *101*, 11068–11076.
- (24) Pyo, S. M.; Shin, T. J.; Kim, S. I.; Ree, M. *Mol. Cryst. Liq. Cryst.* **1998**, *316*, 353–358.
- (25) Matsuda, S.; Urano, Y.; Park, J. W.; Ha, C. S.; Ando, S. *J. Photopolym. Sci. Technol.* **2004**, *17*, 241–246.
- (26) Ishii, J.; Horii, S.; Sensui, N.; Hasegawa, M.; Vladimirov, L.; Kochi, M.; Yokota, R. *High Perform. Polym.* **2009**, *21*, 282–303.
- (27) Takizawa, K.; Wakita, J.; Sekiguchi, K.; Ando, S. *Macromolecules* **2012**, *45*, 4764–4771.
- (28) Kwon, J. E.; Park, S. Y. *Adv. Mater.* **2011**, *23*, 3615–3642.
- (29) Uzhinov, B. M.; Khimich, M. N. *Russ. Chem. Rev.* **2011**, *80*, 553–577.
- (30) Zhao, J.; Ji, S.; Chen, Y.; Guo, H.; Yang, P. *Phys. Chem. Chem. Phys.* **2012**, *14*, 8803–8817.
- (31) Liu, B.; Wang, J.; Zhang, G.; Bai, R.; Pang, Y. *ACS Appl. Mater. Interfaces* **2014**, *6*, 4402–4407.
- (32) Philipova, T.; Ivanova, C.; Kamdzhilov, Y.; Molina, M. T. *Dyes Pigm.* **2002**, *53*, 219–227.
- (33) Piechowska, J.; Huttunen, K.; Wrobel, Z.; Lemmetyinen, H.; Tkachenko, N. V.; Gryko, D. T. *J. Phys. Chem. A* **2012**, *116*, 9614–9620.
- (34) Kim, C. H.; Park, J.; Seo, J.; Park, S. Y.; Joo, T. *J. Phys. Chem. A* **2010**, *114*, 5618–5629.
- (35) Ruckebusch, C.; Sliwa, M.; Rehault, J.; Naumov, P.; Huvenne, J. P.; Buntinx, G. *Anal. Chim. Acta* **2009**, *642*, 228–234.
- (36) Chou, P.; Mcmorrow, D.; Aartsma, T. J.; Kasha, M. *J. Phys. Chem.* **1984**, *88*, 4596–4599.
- (37) Chou, P. T.; Martinez, M. L. *Radiat. Phys. Chem.* **1993**, *41*, 373–378.
- (38) Stein, M.; Keck, J.; Waiblinger, F.; Fluegge, A. P.; Kramer, H. E. A.; Hartschuh, A.; Port, H.; Leppard, D.; Rytz, G. *J. Phys. Chem. A* **2002**, *106*, 2055–2066.
- (39) Xu, Y.; Liu, Q.; Dou, B.; Wright, B.; Wang, J.; Pang, Y. *Adv. Healthcare Mater.* **2012**, *1*, 485–492.
- (40) Tang, K. C.; Chang, M. J.; Lin, T. Y.; Pan, H. A.; Fang, T. C.; Chen, K. Y.; Hung, W. Y.; Hsu, Y. H.; Chou, P. T. *J. Am. Chem. Soc.* **2011**, *133*, 17738–17745.
- (41) Park, S.; Kim, S.; Seo, J.; Park, S. Y. *Macromolecules* **2005**, *38*, 4557–4559.
- (42) Chu, Q.; Medvetz, D. A.; Pang, Y. *Chem. Mater.* **2007**, *19*, 6421–6429.
- (43) Campo, L. F.; Rodembusch, F. S.; Stefani, V. *J. Appl. Polym. Sci.* **2006**, *99*, 2109–2116.
- (44) Lee, S. J.; Jung, J. C.; Lee, S. W.; Ree, M. *J. Polym. Sci., Part A: Polym. Chem.* **2004**, *42*, 3130–3142.
- (45) Oishi, Y.; Ogasawara, K.; Hirahara, H.; Mori, K. *J. Photopolym. Sci. Technol.* **2001**, *14*, 37–40.
- (46) Oishi, Y.; Kikuchi, N.; Mori, K.; Ando, S.; Maeda, K. *J. Photopolym. Sci. Technol.* **2002**, *15*, 213–214.
- (47) Sheldrick, G. M. *Acta Crystallogr., Sect. A* **2008**, *64*, 112–122.
- (48) Lee, C.; Yang, W.; Parr, R. G. *Phys. Rev.* **1988**, *B37*, 785–789.
- (49) Miehlisch, B.; Savin, A.; Stoll, H.; Preuss, H. *Chem. Phys. Lett.* **1989**, *157*, 200–206.
- (50) Becke, A. D. *J. Chem. Phys.* **1993**, *98*, 5648–5652.
- (51) Frisch, M. J.; et al. *Gaussian 09, Revision B.01*; Gaussian, Inc.: Wallingford, CT, 2010.
- (52) Gilli, G.; Bellucci, F.; Ferretti, V.; Bertolasi, V. *J. Am. Chem. Soc.* **1989**, *111*, 1023–1028.
- (53) Bilton, C.; Allen, F. H.; Shields, G. P.; Howard, J. A. K. *Acta Crystallogr.* **2000**, *B56*, 849–856.
- (54) Steiner, T. *Angew. Chem., Int. Ed.* **2002**, *41*, 48–76.
- (55) Houjou, H.; Motoyama, T.; Banno, S.; Yoshikawa, I.; Araki, K. *J. Org. Chem.* **2009**, *74*, 520–529.
- (56) Dreuw, A.; Plotner, J.; Lorenz, L.; Wachtveitl, J.; Djanhan, J. E.; Bruning, J.; Metz, T.; Bolte, M.; Schmidt, M. U. *Angew. Chem., Int. Ed.* **2005**, *44*, 7783–7786.
- (57) Lorenz, L.; Plotner, J.; Matylytsky, V. V.; Dreuw, A.; Wachtveitl, J. *J. Phys. Chem. A* **2007**, *111*, 10891–10898.
- (58) Hanson, K.; Patel, N.; Whited, M. T.; Djurovich, P. I.; Thompson, M. E. *Org. Lett.* **2011**, *13*, 1598–1601.
- (59) Fin, A.; Petkova, L.; Doval, D. A.; Sakai, N.; Vauthey, E.; Matile, S. *Org. Biomol. Chem.* **2011**, *9*, 8246–8252.
- (60) Roberts, E. L.; Dey, J.; Warner, I. M. *J. Phys. Chem. A* **1997**, *101*, 5296–5301.
- (61) Zahid, M.; Grampp, G.; Mansha, A.; Bhatti, I. A.; Asim, S. *J. Fluoresc.* **2013**, *23*, 829–837.